Eur. Phys. J. B **16**, 49–58 (2000)

**THE EUROPEAN PHYSICAL JOURNAL B**

EDP Sciences


# Ab initio study of phonons and structural stabilities of the perovskite-type $MgSiO_3$

K. Parlinski[1,2,a] and Y. Kawazoe[1]

[1] Institute for Materials Research, Tohoku University, 2-1-1 Katahira, Sendai 980-8577, Japan
[2] Institute of Nuclear Physics, ul. Radzikowskiego 152, 31-342 Cracow, Poland

Received 15 October 1999 and Received in final form 14 January 2000

**Abstract.** Using the local-density approximation, calculating the Hellmann-Feynman forces, applying the direct method and deriving the phonon dispersion relations, the stability of the perovskite-like structures of $MgSiO_3$ at $T = 0$ have been studied. The cubic $Pm\bar{3}m$ phase shows a dispersion-less soft phonon branch spreading from the R to M points of the cubic Brillouin zone. This soft branch persists up to high pressures of 150 GPa. The low-symmetry phases I4/mcm and Imma, P4/mbm can be considered as a result of the soft mode condensation at the M and R points, respectively. These phases prove to be unstable at $T = 0$. The experimentally observed Pmnb phase is a consequence of the intersection of Imma and P4/mbm space groups. Thus, it can be regarded as a simultaneous condensation of two soft modes: one at the M and a second at the R high-symmetry points of the cubic Brillouin zone. The phonon dispersion relations of Pmnb show that this phase is stable and its optical phonons appear above 4.0 THz only.

**PACS.** 63.20.-e Phonons in crystal lattices – 71.15.Mb Density functional theory, local density approximation – 91.35.-x Earth's interior structure and properties

## 1 Introduction

Computer programs based on the density functional theory (DTF) provide a powerful tool with which one is now able to optimize a predetermined crystalline structure and to calculate its ground-state energy. However, a search for an unknown stable crystalline structure still remains an open question. Usually one starts the calculations by assuming a hypothetical high-symmetry structure. Such a structure is defined as a supercell with periodic boundary conditions. One way is to optimize this supercell in P1 symmetry allowing the adjustment of the lattice parameters and atomic position. Such optimization is computationally very costly, since the large number of the free parameters which may vary in the minimization process, is equal to the number of atoms in the supercell times three.

In this article we apply another procedure to search for a crystal structure. One starts the DFT calculations from a hypothetical, high-symmetry structure making use of the symmetry imposed by the crystallographic space group. Application of the symmetry elements usually drastically reduces the number of free-parameters. Then, for the structure optimized within the space group one calculates the phonon dispersion relations. If all phonon frequencies $\omega^2(\mathbf{k}, j)$ are positive the structure is stable. However, often this is not the case. If it appears that some phonon frequencies are imaginary, *i.e.* $\omega^2(\mathbf{k}, j) < 0$, then the system is unstable. The most negative mode $\omega^2(\mathbf{k}, j)$ is called the soft mode. The wave vector $\mathbf{k}$, more precisely the irreducible star of the wave vector $\{\mathbf{k}\}$, and the polarization vectors $\mathbf{e}(\mathbf{k}, j)$ of the soft mode components define the lattice distortions and the atomic shifts, which must be performed in order to reach the stable configuration. Moreover, the irreducible representation of the soft mode $\Gamma_\mathrm{s}$, which is uniquely defined by the soft mode wave vectors and polarization vectors, reduces the space group $\mathcal{G}_\mathrm{o}$ of the high-symmetry phase to a space subgroup $\mathcal{G}$ of the low-symmetry phase. This symmetry reduction is unique only if the soft mode is represented by the one-dimensional irreducible representation. More frequently, however, the $\Gamma_\mathrm{s}$ has a higher dimension, and then a subduction with $\Gamma_\mathrm{s}$ leads to a few low-symmetry space groups $\mathcal{G}_1$, $\mathcal{G}_2$, ... $\mathcal{G}_n$, where $n$ is usually of order 2 to 6. Such symmetry analysis suggests the list of space subgroups within which the studied crystalline structure should be optimized. It also assures us that the stable configuration cannot occur within other space groups. (One may, however, start the calculations from another hypothetical structure.) Again, to be sure that the resulting structure is stable, all frequencies of the phonon dispersion relations should be positive. The above procedure considerably reduces the phase space of the possible structures to be searched. In comparison to a single minimization in the P1 structure, in this approach the number of tested structures has increased, but

[a] e-mail: krzysztof.parlinski@ifj.edu.pl

the number of free-parameters involved in the optimization procedures are much smaller. Moreover, the structures exhibiting soft modes become promising candidates for the disordered structures stable at elevated temperature. The described procedure is analogous to the symmetry considerations in the Landau theory of phase transitions, where two crystalline phases are related by the group-subgroup relationship. Below, we illustrate the above procedure considering $MgSiO_3$ perovskite-like structures.

It is believed that magnesium silicate $MgSiO_3$ (with about 10% of the Mg atoms substituted by Fe) is the one of the major constituent components of the Earth's lower mantle. This statement follows from the large cosmic abundance of the elements Mg, Si and O, mass, inertia and density of the Earth and from measurements of speed and polarization of seismic elastic waves. The $MgSiO_3$ properties and phase transitions determine much of the Earth's density distribution and thermal properties [1]. Convection in the upper and lower mantles caused by temperature gradients is another topic under debate [2,3]. The comprehensive description of the physics and chemistry of the deep interior of the Earth, the composition of the mantle and core, the mineral thermodynamics, equation of states and elasticity, the novel physical phenomena at ultrahigh pressures, the high pressure electronic and magnetic properties and the theory of minerals at high pressure including the first-principle approach can be found in the excellent reviews in [4].

$MgSiO_3$ exists in many crystallographic phases. It is believed that under high-pressure $MgSiO_3$ exists in the mantle as a distorted perovskite structure of Pbnm symmetry (equivalent to Pmnb [5]). The Pbnm phase cannot be obtained under normal conditions. It is usually grown at high pressure at about 23 GPa and high temperature [6,7], then recovered by lowering the temperature and subsequently releasing the pressure. On heating at ambient pressure to only modest temperature (150 °C), the crystalline $MgSiO_3$ gradually transforms to a low-density amorphous phase.

The $MgSiO_3$ perovskite has been already studied within the *ab initio* approach. In reference [8] the periodic Hartree-Fock self-consistent field method has been used to describe the equation of states in $MgSiO_3$ perovskite. An *ab initio* constant-pressure molecular-dynamics technique has been used [9] to investigate zero-temperature behaviour of $MgSiO_3$ perovskite up to the pressures which exceed the highest values reached in the Earth's mantle. These studies confirm that $MgSiO_3$ remains in the orthorhombically distorted perovskite phase (Pbnm) up to the highest pressure. Hemley *et al.* [10] have calculated the phonon dispersion curves for $MgSiO_3$ in $Pm\bar{3}m$ cubic symmetry, and have found soft modes at R and M-points of the Brillouin zone. These calculations used a crystal charge density constructed from the shell-stabilized ions, whose wave functions were calculated from the Hartree-Fock theory. The short-range forces were calculated in the pairwise-additive approximation from modified electron gas theory. Stixrude *et al.* [11] have calculated the phonon dispersion curves of $CaSiO_3$ perovskite, using the linearized augmented plane waves method and the linear response approach to the cubic $Pm\bar{3}m$ phase, and found soft modes at the R and M points, and the Born effective charge tensors. Hemmati *et al.* [12] have studied the phase transition from the crystal to the amorphous state in $MgSiO_3$ and $CaSiO_3$ by the rigid-ion pair potential. The phonon dispersion curves of the $MgSiO_3$ were not shown but the dispersion curves of the similar $CaSiO_3$ in the tetragonal phase P4mm exhibit a flat, soft mode along a line connecting M and A high-symmetry points in the tetragonal Brillouin zone. Warren and Ackland [13] have used the density-functional theory and the direct method to derive the phonon frequencies at $\Gamma$, X, M, and R high-symmetry points (with respect to the simple cubic Brillouin zone) of the orthorhombic (Pbnm) and two hypothetical phases: cubic ($Pm\bar{3}m$) and tetragonal (I4/mcm). They have shown that the orthorhombic Pbnm phase is stable and suggested that the tetragonal phase I4/mcm may exist at higher temperature in the lower mantle. Unfortunately, the *ab initio* phonon dispersion relations of the stable orthorhombic Pbnm structure have not yet been calculated. Winkler and Dove [14] have performed the molecular dynamics simulation using the short-range interatomic potentials and conventional Ewald summations with parameters taken from reference [15]. The thermodynamic properties and the phonon density of states have been extracted using a semiclassical approximation. Chaplot *et al.* [16] carried out a molecular dynamics simulation at high temperature and pressures using an empirical potential. At temperatures substantially higher than the mantle temperature, the simulations reveal an orthorhombic to cubic phase transition accompanied by a sharp increase in diffusion of the oxygen atoms.

This work considers a series of perovskite structures which are indicated by the soft modes found in the hypothetically perfectly cubic perovskite phase of $MgSiO_3$. The possible lattice distortions of the perovskite structures have been described in reference [17]. Using the concept of the Landau theory of phase transitions, the symmetry confinement imposed by the group-subgroup relationships, then the density-functional theory and the direct method to calculate harmonic phonons, we study the stability of the distorted perovskite structures predicted by the soft modes. We consider five structures of symmetry $Pm\bar{3}m$, I4/mcm, Imma, P4/mbm and Pmnb. To check the stability of the considered structures we calculate the phonon dispersion curves for each phase. Imaginary frequencies ($\omega^2(\mathbf{k}, j) < 0$), shown as negative values in the figures, represent the soft modes. The wave vector and the irreducible representation of the soft mode lead in each case to lower symmetry phases, which might be candidates for a stable phase. We would like to stress, however, that the soft modes appearing in this work, are used only as hints which tell us in which direction the atoms should be distorted in order to find the stable minimum. This procedure considerably reduces the phase space to be searched. The existence of a crystalline phase with a real soft mode, is a topic going beyond the aim of this article. We have

**Table 1.** Input data used in the *ab initio* calculations of magnesium silicate $MgSiO_3$: orientation of the studied unit cells with respect to the cubic unit cell, supercell's basic vectors, and parameters for *ab initio* calculations.

| Space group | $Pm\bar{3}m$ ($O_h^1$) | $I4/mcm$ ($D_{4h}^{18}$) | $Imma$ ($D_{2h}^{28}$) | $P4/mbm$ ($D_{4h}^{5}$) | $Pmnb$ ($D_{2h}^{16}$) |
|---|---|---|---|---|---|
| Orientation of unit cell | $\mathbf{a}_c = a_o(1,0,0)$<br>$\mathbf{a}_c = a_o(0,1,0)$<br>$\mathbf{c}_c = a_o(0,0,1)$ | $\mathbf{a}_t = a_o(1,\bar{1},0)$<br>$\mathbf{b}_t = a_o(1,1,0)$<br>$\mathbf{c}_t = a_o(0,0,2)$ | $\mathbf{a}_o = a_o(1,0,1)$<br>$\mathbf{b}_o = a_o(0,2,0)$<br>$\mathbf{c}_o = a_o(1,0,\bar{1})$ | $\mathbf{a}_T = a_o(1,\bar{1},0)$<br>$\mathbf{b}_T = a_o(1,1,0)$<br>$\mathbf{c}_T = a_o(0,0,1)$ | $\mathbf{a}_O = a_o(0,0,2)$<br>$\mathbf{b}_O = a_o(1,1,0)$<br>$\mathbf{c}_O = a_o(\bar{1},1,0)$ |
| Supercell | $2 \times 2 \times 2$ | $\sqrt{2} \times \sqrt{2} \times 1$ | $\sqrt{2} \times 1 \times \sqrt{2}$ | $\sqrt{2} \times \sqrt{2} \times 2$ | $\sqrt{2} \times \sqrt{2} \times 1$ |
| Supercell's basic vectors | $\mathbf{a} = 2\mathbf{a}_c$<br>$\mathbf{b} = 2\mathbf{b}_c$<br>$\mathbf{c} = 2\mathbf{c}_c$ | $\mathbf{a} = \mathbf{a}_t + \mathbf{b}_t$<br>$\mathbf{b} = -\mathbf{a}_t + \mathbf{b}_t$<br>$\mathbf{c} = \mathbf{c}_t$ | $\mathbf{a} = \mathbf{a}_o - \mathbf{c}_o$<br>$\mathbf{b} = \mathbf{b}_o$<br>$\mathbf{c} = \mathbf{a}_o + \mathbf{c}_o$ | $\mathbf{a} = \mathbf{a}_T + \mathbf{b}_T$<br>$\mathbf{b} = -\mathbf{a}_T + \mathbf{b}_T$<br>$\mathbf{c} = 2\mathbf{c}_T$ | $\mathbf{a} = \mathbf{c}_O$<br>$\mathbf{b} = \mathbf{a}_O + \mathbf{b}_O$<br>$\mathbf{c} = -\mathbf{a}_O + \mathbf{b}_O$ |
| Number of atoms | 40 | 40 | 40 | 40 | 40 |
| $k$-mesh | $2 \times 2 \times 2$ | $2 \times 2 \times 2$ | $2 \times 2 \times 2$ | $2 \times 2 \times 2$ | $2 \times 2 \times 2$ |
| Number of $k$-points | 4 | 6 | 6 | 6 | 6 |

found that the orthorhombic Pmnb phase is stable and that it is a result of simultaneous condensation of two soft modes, one belonging to the M-point of the cubic Brillouin zone, a second corresponding to the R-point. The unit cell of Pbnm phase contains 20 atoms. For this phase we have calculated, to the best of our knowledge for the first time, the phonon dispersion curves and the phonon density of states, the main characteristics of the crystal dynamics.

## 2 Method

The *ab initio* calculations of $MgSiO_3$ crystals are performed using the pseudopotential method within the local-density approximation (LDA) as implemented in the VASP package [18,19] and with the ultrasoft pseudopotentials provided by VASP. The pseudopotentials for Mg, Si and O atoms represent $s^2p^0$, $s^2p^2$, and $s^2p^4$ electron configurations, respectively. For different phases we use supercells of slightly different shapes, but their forms are close to the $2 \times 2 \times 2$ cubic supercell. Each supercell contains 40 atoms. This choice guarantees that in each case the same neighbours are included into the dynamical matrix. A plane-wave basis set with 500 eV cutoff is used to expand the electronic wave functions at special $k$-points generated by a $2 \times 2 \times 2$ Monkhurst-Pack $k$-mesh, except the elongated $1 \times 1 \times 8$ supercell, for which a $4 \times 4 \times 1$ $k$-mesh has been used.

The phonons are determined by the direct method [20–22], using the optimized supercells subject to symmetry constraints as given in Tables 1 and 2. The Hellmann-Feynman forces are computed for all $n$ independent displacements required by the symmetry of the unit cell as listed in Table 3. The displacement amplitudes are of the order of 0.5% of the lattice constant. The displaced configurations generate $n \times 3 \times 40 = 120n$ components of Hellmann-Feynman forces. The number of force constant matrices and number of independent parameters, as well as the number of coordination shells over which the force constants are spread, are also given in Table 3. Using the symmetry elements of the relevant space group we establish the symmetry of the so-called cummulant force constants [21] and the related number of independent parameters. Using the PHONON program [22] the force constant parameters are fitted to Hellmann-Feynman forces by the singular value decomposition algorithm, which simultaneously provides the least-square solution.

Independent of the range of interaction, the direct method gives exact phonon frequencies at the wave vectors commensurate with the size of the supercell, provided the supercell shape guarantees a complete list of neighbours of each coordination shell such that the dynamical matrix conserves its symmetry. All structures considered in this article satisfy this condition. In Table 2 we list the details of these structures. In particular we show the special wave vectors at which phonon frequencies are obtained exactly for a given supercell. Since in $MgSiO_3$ the magnitude of the force constants diminishes with distance rather rapidly, all phonon branches, being a symmetry controlled interpolation between special wave vectors, should be relatively well reproduced.

In $MgSiO_3$ the macroscopic electric field splits the infrared active optical modes to transverse (TO) and longitudinal (LO) components. The TO phonon frequencies are calculated within the direct method. The LO modes depend on the non-analytical term [23], which generally depends on the ratio of the effective charge tensor to the square root of the dielectric constant $\mathbf{Z}_i^*/\sqrt{\epsilon_\infty}$. Further, we treat the effective charges as point charges. Using the direct method the LO modes can be estimated from an elongated supercell [24], since such a supercell provides exact phonons inside the Brillouin zone as well. For that we build a $1 \times 1 \times 8$ supercell of the cubic $Pm\bar{3}m$ symmetry elongated along the $z$ direction with 40 atoms. Its optimized ground state energy and the lattice constants are the same as in the optimized $2 \times 2 \times 2$ cubic supercell. We calculate the Hellmann-Feynman forces and derive the dispersion curves along the $\Gamma$–Z direction. This supercell provides correct phonon frequencies at four wave vectors: $(0,0,\frac{1}{8})$, $(0,0,\frac{1}{4})$, $(0,0,\frac{3}{8})$, $(0,0,\frac{1}{2})$. The phonon frequencies at these wave vectors are used to extrapolate the LO branch towards the $\Gamma$ point and to estimate

**Table 2.** Data obtained from the *ab initio* calculations of magnesium silicate $MgSiO_3$: wave vectors at which the exact phonon frequencies follow from the direct method, optimized zero-pressure lattice constants, difference $\Delta E = E - E_c$ of ground state energy in eV per cubic unit cell ($Z = 1$) with respect to the cubic ground state energy $E_c$, reduced unit cell volumes $V/Z$ corresponding to original perovskite ($Z = 1$) unit cell, optimized zero-pressure structural parameters. Experimental lattice constants of Pmnb orthorhombic phase are $a = 6.9083(8)$, $b = 4.9313(4)$, $c = 4.7787(4)$, and measured atomic positions are Si:$(0, 0, 1/2)$, Mg:$(0.5560(1), 1/4, 0.5141(1))$, O1:$(0.4660(2), 1/4, 0.1028(2))$, O2:$(0.2014(4), 0.5531(4), 0.1961(1))$ [29]. (see also [30,31]).

| Space group | $Pm\bar{3}m$ ($O_h^1$) | I4/mcm ($D_{4h}^{18}$) | Imma ($D_{2h}^{28}$) | P4/mbm ($D_{4h}^{5}$) | Pmnb ($D_{2h}^{16}$) |
|---|---|---|---|---|---|
| Exact phonons at | $\Gamma$, X, M, R | $\Gamma$, X, Z | $\Gamma$, X, R | $\Gamma$, M, Z, A | $\Gamma$, T |
| Lattice constants in Å | $a = 3.4596$ | $a = 4.8242$<br>$c = 6.9224$ | $a = 4.9037$<br>$b = 6.8626$<br>$c = 4.7421$ | $a = 4.8194$<br>$c = 3.4663$ | $a = 6.8062$<br>$b = 4.8751$<br>$c = 4.7093$ |
| $Z$ | 1 | 2 | 2 | 2 | 4 |
| $\Delta E$ | 0.0 | $-0.7674$ | $-1.1757$ | $-0.7611$ | $-1.4269$ |
| Volume $V/Z$ in Å | 41.4073 | 40.2701 | 38.8954 | 40.2552 | 39.0647 |
| Atomic positions | Si:$(0, 0, 0)$<br>Mg:$(\frac{1}{2}, \frac{1}{2}, \frac{1}{2})$<br>O:$(\frac{1}{2}, \frac{1}{2}, 0)$ | Si:$(0, 0, 0)$<br>Mg:$(\frac{1}{2}, 0, \frac{3}{4})$<br>O1:$(0, 0, \frac{3}{4})$<br>O2:$(u, v, 0)$<br>$u = 0.1819$<br>$v = \frac{1}{2} - u$ | Si:$(0, 0, \frac{1}{4})$<br>Mg:$(0, \frac{1}{4}, u)$<br>O1:$(0, \frac{1}{4}, v)$<br>O2:$(\frac{1}{4}, t, \frac{1}{4})$<br>$u = 0.4688$<br>$v = 0.8817$<br>$t = 0.0625$ | Si:$(0, 0, \frac{1}{2})$<br>Mg:$(\frac{1}{2}, 0, 0)$<br>O1:$(0, 0, 0)$<br>O2:$(u, v, \frac{1}{2})$<br>$u = 0.3182$<br>$v = \frac{1}{2} - u$ | Si:$(0, 0, \frac{1}{2})$<br>Mg:$(u, \frac{1}{4}, v)$<br>O1:$(t, \frac{1}{4}, w)$<br>O2:$(x, y, z)$<br>$u = 0.5596$<br>$v = 0.5149$<br>$t = 0.4623$<br>$w = 0.1083$<br>$x = 0.1992$<br>$y = 0.5559$<br>$z = 0.1935$ |

**Table 3.** Displacements used to generate Hellmann-Feynman (HF) forces, number of Hellmann-Feynman force components, number of coordination shells within the supercell, number of the force constant matrices and number of independent parameters appearing in the force constant matrices used in the calculations.

| Space group | $Pm\bar{3}m$ ($O_h^1$) | I4/mcm ($D_{4h}^{18}$) | Imma ($D_{2h}^{28}$) | P4/mbm ($D_{4h}^{5}$) | Pmnb ($D_{2h}^{16}$) |
|---|---|---|---|---|---|
| Displacements to generate HF forces | Mg: $z$<br>Si: $z$<br>O: $x$,$z$ | Mg: $x$,$z$<br>Si: $x$,$z$<br>O1: $x$,$z$<br>O2: $x$,$y$,$z$ | Mg: $x$,$y$,$z$<br>Si: $x$,$y$,$z$<br>O1: $x$,$y$,$z$<br>O2: $x$,$y$,$z$ | Mg: $x$,$z$<br>Si: $x$,$z$<br>O1: $x$,$z$<br>O2: $x$,$y$,$z$ | Mg: $x$,$y$,$z$<br>Si: $x$,$y$,$z$<br>O1: $x$,$y$,$z$<br>O2: $x$,$y$,$z$ |
| HF forces | 480 | 1080 | 1440 | 1080 | 1440 |
| Coordinat. shells | 9 | 20 | 26 | 19 | 37 |
| Force constants | 22 | 45 | 63 | 44 | 78 |
| Independ. param. | 49 | 228 | 382 | 210 | 616 |

the ratios of the point effective charges to the square root of the dielectric constant, which are $Z^*_{Mg}/\sqrt{\epsilon_\infty} = 1.0$, $Z^*_{Si}/\sqrt{\epsilon_\infty} = 2.0$ and $Z^*_{O}/\sqrt{\epsilon_\infty} = -1.0$. Here, the ratio between effective charges is assumed to be the same as the ratio between nominal static charges. We use these ratios for all selected structures. We remark, however, that all studied soft modes are not influenced by the LO/TO splitting. Hence, the stabilities of the considered structures do not depend on the effective charges.

## 3 Cubic perovskite structure of magnesium oxide

We start the calculation from the cubic perovskite $MgSiO_3$ phase. Therefore, we have constructed a $2 \times 2 \times 2$ supercell of $Pm\bar{3}m$ symmetry, optimized its lattice constant, calculated the Hellmann-Feynman forces and derived the phonon dispersion curves along high-symmetry

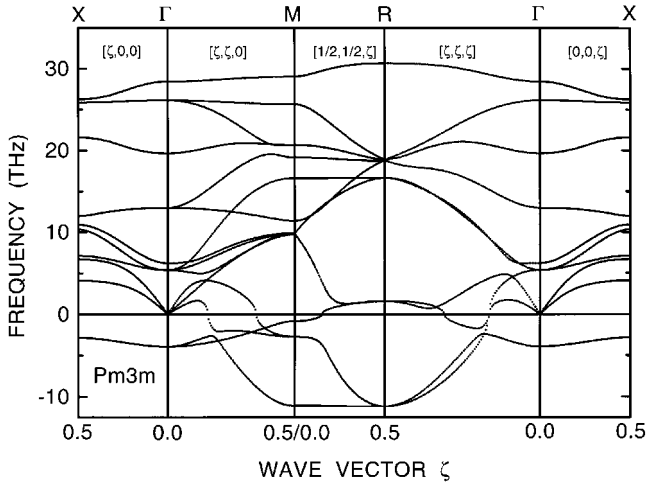


**Fig. 1.** Phonon dispersion relations of $MgSiO_3$ for the cubic perovskite $Pm\bar{3}m$ phase.

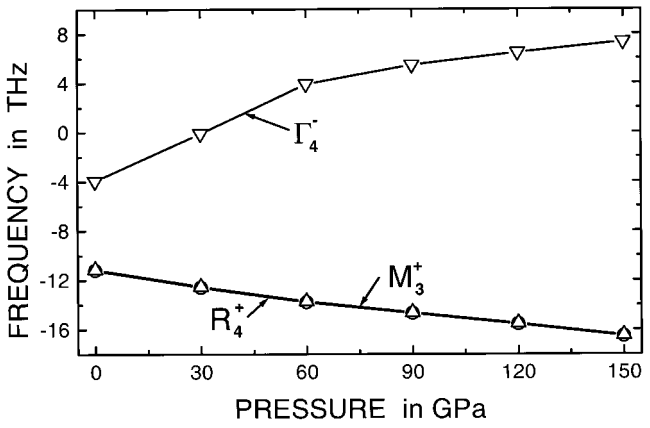


**Fig. 2.** Pressure dependence of the soft modes in the $Pm\bar{3}m$ structure.

directions. The results are shown in Figure 1. Out of 15 phonon branches several are soft. At the R: $(\frac{1}{2},\frac{1}{2},\frac{1}{2})$ point the triply degenerate mode $R_4^+$ [25] (or $k_{13}\tau^9$ [26]) has the lowest frequency. The mode $M_3^+$ [25] (or $k_{11}\tau^3$ [26]) at M: $(\frac{1}{2},\frac{1}{2},0)$ point has practically the same frequency. A phonon branch along the $[\frac{1}{2},\frac{1}{2},\zeta]$ direction remains dispersion-less and soft between R and M points. The flatness of this dispersion curve is caused by the small value of the latteral oxygen-oxygen force constant at the lattice constant $a$ distance, which amounts to only 0.6% of the on-site oxygen force constant. There are, of course, no symmetry requirements which force this dispersion curve to be flat. We add that a similar relatively flat dispersion curve occurs in other perovskites like $SrTiO_3$, where the flatness along the R–M direction has been confirmed experimentally [27].

In cubic $MgSiO_3$ we observe another soft mode at the $\Gamma$ point, shown in Figure 1. Its symmetry is $T_{1u}(\mathrm{TO})$, and its frequency $i3.95$ THz. From the symmetry point of view, this soft mode might, in principle, induce a P4mm phase. The P4mm phase could become ferroelectric. But, since the $T_{1u}(\mathrm{TO})$ soft mode frequency is considerably higher than the frequencies of modes arising from the R or M points, the $T_{1u}$ mode is expected not to cause any effect.

### 3.1 The cubic perovskite structure under pressure

The phonon dispersion curves of the cubic $Pm\bar{3}m$ phase has been evaluated at several hydrostatic pressures up to 150 GPa. Generally, the phonon frequencies increase with increasing pressure. Figure 2 shows the pressure dependence of the soft mode frequencies at the R and M points, which lower with pressure. It indicates that the orthorhombic Pmnb phase will become more distorted from the cubic phase when increasing the pressure. This is contrary to the soft mode $T_{1u}(\mathrm{TO})$ at the $\Gamma$ point, which increases with pressure. Hence, the P4mm phase is not expected to become stable at high pressures.

### 3.2 Symmetry relationships

An irreducible representation of a soft mode induces a list of space subgroups. Such group-subgroup relationships provide the unit cells of low symmetry phases, and the mutual orientations of the parent and resulting phases. Furthermore, since one knows the polarization vector of the soft mode in the parent phase, one may displace atoms to directions indicated by the calculated polarization vector, and hence distort the parent structure towards the resulting one. Only the displacement amplitudes and the new lattice constants require optimization.

The $Pm\bar{3}m$ cubic structure of $MgSiO_3$ is considered as a parent phase. The $Pm\bar{3}m$ space group can be lowered by the irreducible representations of the soft modes according to the following subduction diagrams [25]:

$$\begin{aligned} \mathrm{Pm}\bar{3}\mathrm{m}(Z=1) &\to (R_4^+, e_1=e_2\neq 0,\, e_3=0) \\ &\to \mathrm{Imma}(Z=2) \end{aligned} \tag{1}$$

$$\begin{aligned} \mathrm{Pm}\bar{3}\mathrm{m}(Z=1) &\to (R_4^+, e_1=e_2=0,\, e_3\neq 0) \\ &\to \mathrm{I4/mcm}(Z=2) \end{aligned} \tag{2}$$

$$\begin{aligned} \mathrm{Pm}\bar{3}\mathrm{m}(Z=1) &\to (M_3^+, \mathbf{k}_{xz}^{(\mathrm{M})}=\mathbf{k}_{yz}^{(\mathrm{M})}=0, \mathbf{k}_{xy}^{(\mathrm{M})}\neq 0) \\ &\to \mathrm{I4/mbm}(Z=2). \end{aligned} \tag{3}$$

There is only one arm of the irreducible star of the representation $R_4^+$ of $Pm\bar{3}m$. The ray representation of $R_4^+$ is three-dimensional. Hence, the order parameter has three components. In the first case, equation (1), two equal components of the $R_4^+$ order parameter condense, while in the second case, equation (2), only one component of $R_4^+$ is involved. The irreducible star of M point consists of three arms, but the relevant ray representation $M_3^+$ is one-dimensional. The symmetry reduction, equation (3), is due to a condensation of a single arm $\mathbf{k}_{xy}^{(\mathrm{M})}$ of the M irreducible star. Except for the above mentioned low-symmetry phases, there are a few other possibilities. However at the moment, we limit the discussion to the above three space groups, since only these are necessary to consider for the stable orthorhombic Pmnb phase.

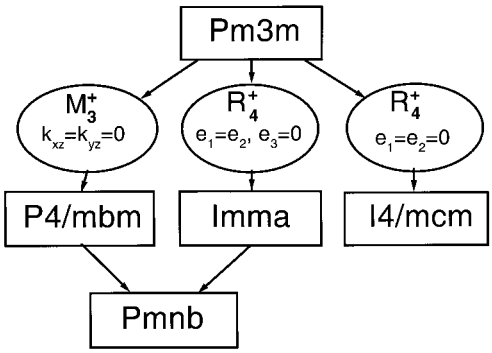


**Fig. 3.** Space group relationships of the $MgSiO_3$ structures studied in this article. The $Pm\bar{3}m$ is the parent perovskite structure. The Imma and I4/mcm, and P4/mbm space groups are the subgroups of $Pm\bar{3}m$, induced by irreducible representations labelled by wave vectors of the high-symmetry points R, and M, respectively. The orthorhombic space group Pmnb = P4/mbm ∩ Imma contains common symmetry element of P4/mbm and Imma space groups. The Pmnb space group is equivalent to Pbnm one [5].

The group-subgroup relationships are shown in Figure 3. There one sees that the common symmetry elements of one space group from the R point and of the space group from the M point create another orthorhombic space group Pmnb. Hence, their intersection gives

$$\mathrm{P4/mbm}\,(Z=2) \cap \mathrm{Imma}\,(Z=2) = \mathrm{Pmnb}\,(Z=4). \quad (4)$$

The Pmnb phase is a result of simultaneous condensation of the two mentioned soft modes, one at the R and a second at the M point.

## 4 Phonon dispersion curves of low-symmetry phases

We have built up supercells (see Tabs. 1, 2 and 3) corresponding to low-symmetry space groups of I4/mcm, Imma, P4/mbm and Pmnb. The structures are optimized at zero-pressure. The resulting lattice constants, unit cell volumes, atomic positions and ground state energies are collected in Table 2. Using these optimized structures, the Hellmann-Feynman forces are calculated for the displacements listed in Table 3. Note the rather large number of independent force constant's parameters. The force constants are fitted to the Hellmann-Feynman forces. Their values diminish with distance between involved atoms. The largest ones are the on-site (zero-distance) constants. The force constant elements at the supercell surfaces are two orders of magnitude smaller than the on-site ones. Such a decrease of the force constants as a function of a distance is quite sufficient to get phonon frequencies at all wave vectors with an appreciable accuracy. We remind the reader that according to the direct method, the phonon frequencies at special $k$-points, listed in Table 2, are obtained exactly, even if the interaction range exceeds the supercell size.

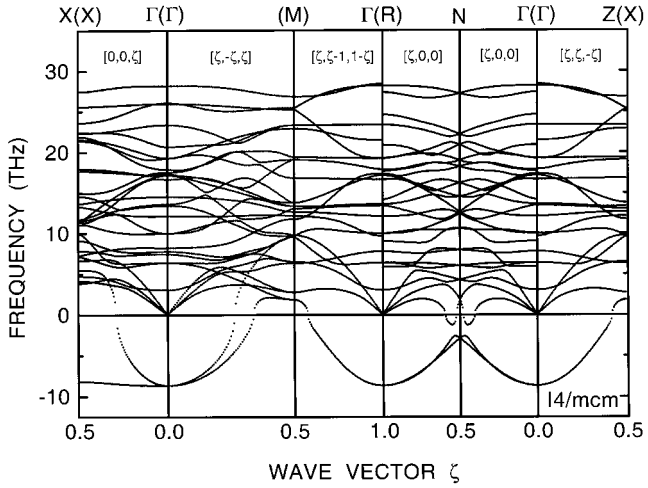


**Fig. 4.** Phonon dispersion relations of $MgSiO_3$ for the body-centered tetragonal I4/mcm structure.

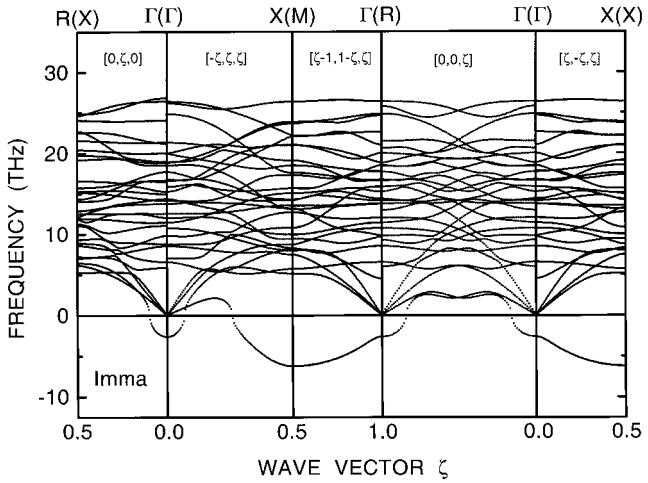


**Fig. 5.** Phonon dispersion relations of $MgSiO_3$ for the body-centered orthorhombic Imma structure.

Figures 4–7 show the phonon dispersion relations. All these curves are calculated along the same high-symmetry lines of the reciprocal lattices. We use the conventional notation for the high-symmetry points in a given Brillouin zone [28]. However, in brackets we quote the corresponding high-symmetry point of the cubic Brillouin zone, from which a given high-symmetry point of the low-symmetry phase arises. Such a presentation of the dispersion curves allows comparison of phonons in different reciprocal lattices. The notation of reciprocal lattice directions in Figures 1 and 4–7 are given in terms of the reciprocal lattice vectors defined in Table 4. The majority of studied crystals exhibit soft modes. Their values are given in Table 5.

### 4.1 Low-symmetry phase I4/mcm

The structural data of the supercell optimized within the constraints of the I4/mcm space group are given in

**Table 4.** Reciprocal lattice vectors $\mathbf{g}_1$, $\mathbf{g}_2$, $\mathbf{g}_3$ (in $\text{Å}^{-1}$) of the studied structures. Any wave vector $\mathbf{k}$ can be expressed as $\mathbf{k} = q_1\mathbf{g}_1 + q_2\mathbf{g}_1 + q_3\mathbf{g}_3$, where $(q_1, q_2, q_3)$ are the wave numbers. The lattice directions shown in Figures 1 and 4–7 on the phonon dispersion relations are given in terms of $(q_1, q_2, q_3)$.

| Space group | $\mathbf{g}_1$ | $\mathbf{g}_2$ | $\mathbf{g}_3$ |
|---|---|---|---|
| $Pm\bar{3}m$ | (0.2891, 0.0000, 0.0000) | (0.0000, 0.2891, 0.0000) | (0.0000, 0.0000, 0.2891) |
| I4/mcm | (0.0000, 0.2073, 0.1445) | (0.2073, 0.0000, 0.1445) | (0.2073, 0.2073, 0.0000) |
| Imma | (0.0000, 0.1457, 0.2109) | (0.2039, 0.0000, 0.2109) | (0.2039, 0.1457, 0.0000) |
| P4/mbm | (0.2075, 0.0000, 0.0000) | (0.0000, 0.2075, 0.0000) | (0.0000, 0.0000, 0.2885) |
| Pbnm | (0.1469, 0.0000, 0.0000) | (0.0000, 0.2051, 0.0000) | (0.0000, 0.0000, 0.2123) |

**Table 5.** Soft mode frequencies in THz and the high-symmetry points at which the soft modes occur. In brackets are given the symbols of high-symmetry points of the original simple cubic Brillouin zone.

| Space group | $Pm\bar{3}m$ ($O_h^1$) | I4/mcm ($D_{4h}^{18}$) | Imma ($D_{2h}^{28}$) | P4/mbm ($D_{4h}^{5}$) | Pmnb ($D_{2h}^{16}$) |
|---|---|---|---|---|---|
| High-symmetry point | R, M | $\Gamma$ (R) | X(M) | Z(R) | None |
| Frequency in THz | $i11.20$, $i11.13$ | $i8.67$ | $i6.23$ | $i9.42$ | None |

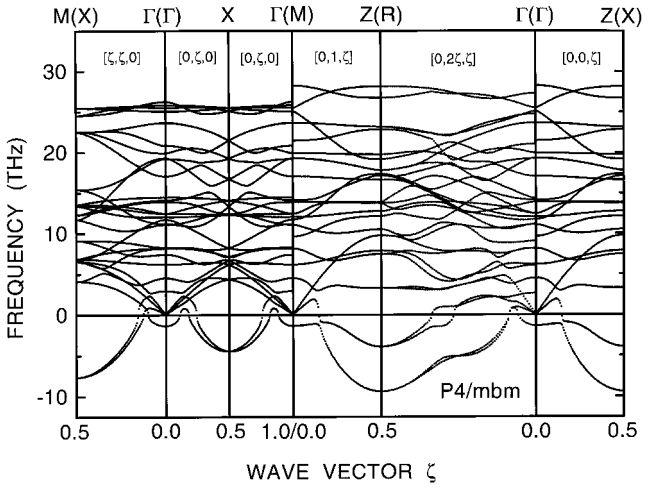


**Fig. 6.** Phonon dispersion relations of $MgSiO_3$ for the tetragonal P4/mbm structure.

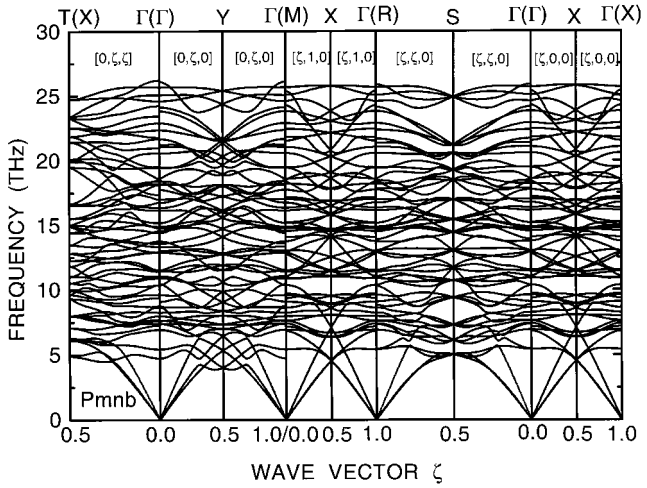


**Fig. 7.** Phonon dispersion relations of $MgSiO_3$ for the stable orthorhombic Pmnb phase [4].

Table 2. Its ground state energy is only $-0.7674$ eV/per cubic unit cell lower then that of the cubic perovskite structure. The phonon dispersion relations have also been calculated. They indicate that the I4/mcm phase is still unstable, since it possesses a soft mode of $E_g$ symmetry at the $\Gamma$ point, shown in Figure 4. This soft mode can further lower the symmetry to $C2/c$ ($C_{2h}^6$) ($Z = 2$), or $C2/m$ ($C_{2h}^3$) ($Z = 2$), or $P\bar{1}$ ($C_i^1$) ($Z = 2$) space groups. However, we have not explored these possibilities, since they do not lead to the Pmnb phase found stable in this work, and suggested by the experiment.

### 4.2 Low-symmetry phases Imma and P4/mbm

The structural data of the supercells optimized under constraints of the Imma and P4/mbm space groups are given in Table 2. The phases Imma and P4/mbm are the results of the condensation of the soft modes at the R and M points of the cubic Brillouin zone, respectively, equations (1, 3). The ground state energy of the Imma structure is considerably lower, than that of P4/mbm. The phonon dispersion relations are calculated and shown in Figures 5 and 6, respectively. Both figures still contain soft modes. However, the Imma crystal, which is a result of the condensation of a soft mode at the R point, shows a soft mode at the X point of the body-centered orthorhombic Brillouin zone. This X point originates from the M point of the cubic Brillouin zone. Thus, the Imma phase has a tendency to deform further.

The reverse situation is observed in the P4/mbm phase. There, the P4/mbm structure arises as a result of the condensation of a soft mode at the M point in

the cubic Brillouin zone. The P4/mbm phase still contains a soft mode at the Z point in the tetragonal Brillouin zone, which corresponds to the R point in the cubic Brillouin zone. Therefore, the P4/mbm phase can further distort. The two soft modes, one at the R point, second at the M point drive the cubic $MgSiO_3$ crystal to the orthorhombic Pmnb structure.

### 4.3 Stable orthorhombic Pmnb phase

The optimized Pmnb structure is stable and it is distorted from the cubic symmetry mainly by tilting the $SiO_6$ octahedra. The Si atom is surrounded by six oxygens in octahedral coordination with bond lengths 1.7679, 1.7808 and 1.7861 Å, and bond angles 89.35°, 88.40° and 88.41°, respectively. The small variations in the Si–O distance and the small departure of the O–Si–O angles from $90^0$ show that the $SiO_6$ octahedron is quite regular. We reproduce the observed structure very well. Our calculated lattice constants and atomic positions are in good agreement with the measured data [29–31] (see Tab. 2). The calculated mean Si–O bond length of 1.7783 Å shows excellent agreement with the experimentally observed value of 1.783 Å [29].

The calculated zero-pressure phonon dispersion relations of the stable orthorhombic Pmnb crystal are shown in Figure 7. The striking feature is that the optic modes are limited to the frequency interval 4.0−26.2 THz. Below 4.0 THz only acoustic modes are present. The discontinuities seen at the $\Gamma$ point are due to the LO/TO splitting. By symmetry all modes are singly degenerate. In Table 6 we give the optic phonon frequencies corresponding to the $\Gamma$ point. The $A_g$, $B_{1g}$, $B_{2g}$ and $B_{3g}$ modes are Raman active, while the transverse optic phonons $B_{1u}$(TO), $B_{2u}$(TO) and $B_{3u}$(TO) are infrared active. The frequencies of the longitudinal components $B_{1u}$(LO), $B_{2u}$(LO) and, $B_{3u}$(LO) are not given in Table 6. The Raman scattering measurements [7,32–35] provide the phonon frequencies, however, the experimental symmetries of these modes have not been established. Therefore, we cannot assign the modes uniquely and we have not performed it.

For completeness of the lattice dynamics we show in Figure 8 the total and partial phonon density of states for Mg, Si and O atoms. The spectra are normalized to 1, $\frac{1}{5}$, $\frac{1}{5}$ and $\frac{3}{5}$, respectively. Figure 8 shows below 4.0 THz an exceptionally low density of states. This means that in this region the acoustic modes contribute very little to the phonon density of states. The Si and O atoms vibrate in the modes of the same frequencies. However, the Mg atoms vibrate preferentially at lower frequencies, although the mass of Mg is only slightly lower than that of Si. This effect is a direct consequence of the strong Si–O bonding, and weaker coupling to Mg atoms. Qualitatively similar phonon density of states have been obtained from the molecular dynamics simulation at $T = 300$ K [14] using phenomenological potentials. The frequency intervals of the distributions are the same. All density of states start at about 4 THz and vanish above 26 THz. The partial density of states for Mg has a very low intensity above 16 THz.

**Table 6.** Phonon symmetries and frequencies at the $\Gamma$ point for orthorhombic Pmnb phase of $MgSiO_3$ at zero pressure. Longitudinal mode frequencies $B_{1u}$(LO), $B_{2u}$(LO), $B_{3u}$(LO) are not listed.

| | | | |
|---|---|---|---|
| $B_{3u}$(TO) | 4.72 | $B_{3g}$ | 14.75 |
| $A_u$ | 5.41 | $A_u$ | 14.84 |
| $B_{2g}$ | 6.91 | $A_g$ | 14.85 |
| $B_{2u}$(TO) | 7.16 | $B_{1u}$(TO) | 15.15 |
| $A_g$ | 7.39 | $B_{2u}$(TO) | 15.19 |
| $A_u$ | 7.60 | $B_{2g}$ | 16.11 |
| $B_{1u}$(TO) | 7.62 | $B_{1g}$ | 16.32 |
| $B_{3g}$ | 7.96 | $A_g$ | 16.72 |
| $A_g$ | 8.23 | $B_{1u}$(TO) | 16.98 |
| $B_{1g}$ | 8.60 | $B_{1u}$(TO) | 17.72 |
| $B_{3u}$(TO) | 8.74 | $B_{3u}$(TO) | 18.10 |
| $B_{1u}$(TO) | 9.07 | $B_{2u}$(TO) | 18.18 |
| $B_{3g}$ | 9.59 | $B_{3g}$ | 18.37 |
| $B_{2u}$(TO) | 9.70 | $A_u$ | 18.50 |
| $B_{1g}$ | 10.35 | $B_{2g}$ | 18.56 |
| $A_g$ | 10.87 | $A_g$ | 19.44 |
| $B_{3g}$ | 10.97 | $B_{3g}$ | 19.47 |
| $A_u$ | 11.02 | $A_u$ | 20.55 |
| $B_{2u}$(TO) | 11.40 | $B_{1u}$(TO) | 21.02 |
| $A_u$ | 11.47 | $B_{3u}$(TO) | 21.64 |
| $A_g$ | 11.52 | $B_{3u}$(TO) | 22.33 |
| $B_{2u}$(TO) | 12.77 | $B_{2u}$(TO) | 22.43 |
| $B_{1g}$ | 12.86 | $A_u$ | 22.87 |
| $B_{2g}$ | 12.88 | $B_{1u}$(TO) | 23.79 |
| $B_{1u}$(TO) | 13.00 | $B_{2u}$(TO) | 24.24 |
| $B_{3u}$(TO) | 13.55 | $B_{1g}$ | 24.56 |
| $B_{1u}$(TO) | 13.73 | $B_{3g}$ | 25.04 |
| $B_{3u}$(TO) | 14.38 | $B_{2g}$ | 25.64 |
| $B_{2u}$(TO) | 14.53 | | |

## 5 Discussion

We have presented the *ab initio* calculations of the structural and dynamical properties of the distorted perovskite structures of $MgSiO_3$. Four derivatives from cubic perovskite structures were checked against stability, using the phonon dispersion relations. This analysis assures us that the experimentally observed Pmnb structure is a result of the condensation of two soft modes, one at the M, and a second at the R point of the cubic Brillouin zone. The soft mode at the M point leads to the P4/mbm unstable structure where the $SiO_6$ octahedra are rotated around the $z$-axis by 15.3 degrees. The soft mode at the R point, in turn, reduces the symmetry to the Imma unstable

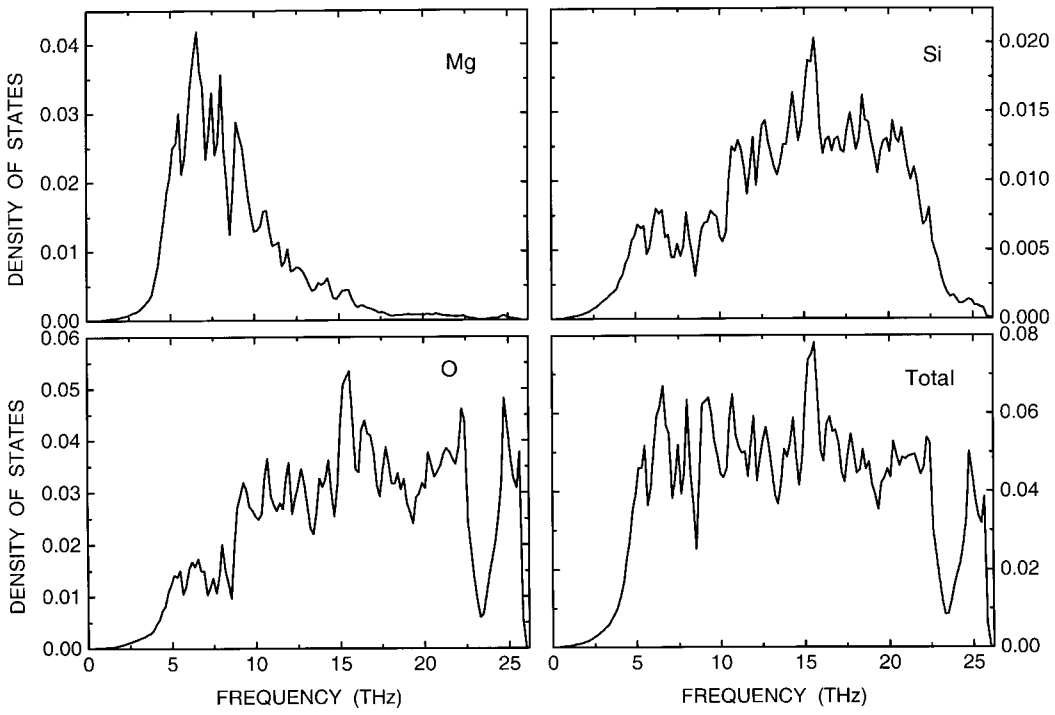


**Fig. 8.** Total and partial phonon density of states for Mg, Si and O atoms. The spectra are normalized to 1 and $\frac{1}{5}$, $\frac{1}{5}$, $\frac{3}{5}$, respectively.

structure, by rotating the $SiO_6$ octahedra around $x$ and $y$ axes. Such a $SiO_6$ rotation is coupled to the lattice strain and causes 5.8% reduction of the crystal volume.

The phases Imma, I4/mcm, P4/mbm and $Pm\bar{3}m$ are also good candidates to become stable disordered phases at elevated temperatures. The orthorhombic Pmnb phase has the lowest ground state energy. The smallest ground state energy excess of 0.2512 eV per cubic unit cell (583 K/atom) occurs for the Imma phase. For the tetragonal I4/mcm and P4/mbm phases these excesses of energies are three times higher. If a transformation from the Pmnb phase to the remaining phases should occur, then all these phase transitions will be of a displacive type. This assertion follows from the fact that in all studied structures the local atomic potentials possess a single minimum. We see this effect, since all the on-site force constants, transformed to a diagonal form, consist of positive parameters only. A disordered phase would require local potential with two, or more local minima. In this case some curvatures of the local potentials, which are equal to the on-site force constants, will be negative.

The calculated phonon dispersion relations, which contain the soft modes and correspond to the unstable phases, have as a rule slightly higher maximal optic phonon frequencies. These modes correspond to the internal vibrations of the $SiO_6$ octahedra. Indeed, the unstable phases remain in a strained state kept by the imposed symmetry elements, and hence the vibrational frequencies slightly increase.

The calculations for the cubic phase disclose along the R–M line of the cubic Brillouin zone a dispersion-less soft branch. Such a behaviour has already been noticed in the phenomenological calculation of $CaSiO_3$ [12]. This property could lead to a number of high-commensurate phases with coexisting different characteristic modulation wave vectors. The precise pathway of such a transition will be sensitive to the anharmonic interactions and to the stress field and temperature of the sample. This topic remains open.

One of us (K.P.) would like to express his thanks to the staff of the Laboratory of Materials Design by Computer Simulation, Institute of Materials Research, Tohoku University, for their great hospitality and assistance during his stay. This work was partially supported by the State Committee of Scientific Research (KBN), grant No. 2 PO3B 004 14.

## References

1. C.R.A Catlow, G.D. Price, Nature **347**, 243 (1990).
2. M.S.T. Bukowinski, G.H. Wolf, *Structural and magnetic phase transitions in minerals*, edited by S.G. Ghose, J.M.D. Coey, E. Salje (Springer-Verlag, New York, 1988), p. 91.
3. R. Jeanloz, S. Morris, Ann. Rev. Earth Planet Sci. **14**, 377 (1986).
4. *Ultra High-Pressure Mineralogy. Physics and Chemistry of the Earth's Deep Interior*, edited by R.J. Hemley, Rev. Mineral. **37** (1998).
5. Instead of Pbnm space group we use thorough the article the setting of Pmnb space group, since it follows from the intersection of two other space groups studied in

this article. The Pmnb is related with Pbnm space group by transformation $(z+\frac{1}{4}, y+\frac{1}{4}, x)$.
6. L.-G. Liu, Geophys. Rev. Lett. **1**, 277 (1974).
7. D.J. Durben, G.H. Wolf, Am. Mineral. **77**, 890 (1992).
8. Ph. D'Arco, G. Sandrone, R. Dovesi, R. Orlando, V.R. Saunders, Phys. Chem. Minerals **20**, 407 (1993).
9. R.M. Wentzcovitch, N.L. Ross, G.D. Price, Phys. Earth Planet. Inter. **90**, 101 (1995).
10. R.J. Hemley, M.D. Jackson, R.G. Gordon, Phys. Chem. Minerals **14**, 2 (1987).
11. L. Stixrude, R.E. Cohen, R. Yu, K. Krakauer, Am. Mineral. **81**, 1293 (1996).
12. M. Hemmanti, A. Chizmeshya, G.H. Wolf, P.H. Poole, J. Shao, C.A. Angell, Phys. Rev. **51**, 14 841 (1995).
13. M.C. Warren, G.J. Ackland, Phys. Chem. Minerals **23**, 107 (1996).
14. B. Winkler, M. Dove, Phys. Chem. Minerals **18**, 407 (1992).
15. M. Matsui, Phys. Chem. Minerals **16**, 234 (1988).
16. S.L. Chaplot, N. Choudhury, K.R. Rao, Amer. Mineralogist **83**, 937 (1998).
17. A.M. Glazer, Acta Cryst. B **28**, 3384 (1972).
18. G. Kresse, J. Hafner, Phys. Rev. B **47**, 558 (1993); *ibid.* **49**, 14 251 (1994).
19. G. Kresse, J. Furhmüller, Software VASP, Vienna (1999); Phys. Rev. B **54**, 11 169 (1996); Comput. Mat. Science **6**, 15 (1996).
20. K. Parlinski, Z.Q. Li, Y. Kawazoe, Phys. Rev. Lett. **78**, 4063 (1997).
21. K. Parlinski, *Neutrons and numerical methods* $N_2M$, edited by M.R. Johnson, G.J. Kearley, H.G. Büttner, Am. Inst. Phys. Conf. Proc. **479**, 121 (1999).
22. K. Parlinski, Software PHONON (1999).
23. R.M. Pick, M.H. Cohen, R.M. Martin, Phys. Rev. B **1**, 910 (1970); A.A. Maradudin, *Elements of the Theory of Lattice Dynamics*, in *Dynamical Properties of Solids*, edited by G.K. Horton, A.A. Maradudin (North-Holland Publishing Company - Amsterdam, 1974), Vol. 1, p. 3.
24. K. Parlinski, J. Łażewski, Y. Kawazoe, J. Phys. Chem. Solids **61**, 87 (1999).
25. H.T. Stockes, D.M. Hatch, *Isotropic Subgroups of the 230 Crystallographic Space Groups* (World Scientific Publishing Co., Teaneck, London, 1988).
26. O.V. Kovalev, *Irreducible Representations of the Space Groups* (Gordon and Breach, New York, 1965).
27. B.G. Stirling, J. Phys. C **5**, 2711 (1972).
28. C.J. Bradley, A.P. Cracknell, *The mathematical theory of symmetry in solids* (Oxford, Clarendon Press, 1972).
29. H. Horiuchi, E. Ito, D. Weidner, Am. Mineral. **72**, 357 (1987).
30. E. Ito, Y. Matsui, Earth Planet Sci. Lett. **38**, 443 (1978).
31. Y. Kudoh, E. Ito, H. Takeda, Phys. Chem. Minerals **14**, 350 (1987).
32. L.-G. Liu, T.P. Mernagh, T. Irifune, J. Phys. Earth **42**, 411 (1994).
33. L.-G. Liu, T.P. Mernagh, T. Irifune, J. Phys. Chem. Solids **55**, 185 (1994).
34. Q. Wiliams, R. Jeanloz, P. McMillan, J. Geophys. Res. **92**, 8116 (1987).
35. R.J. Hemley, R.E. Cohen, A. Yeganeh-Haeri, H.K. Mao, D.J. Weidner, E. Ito, *A Structure of Great Interest to Geophysics and Materials Science*, edited by A. Navrotsky, D.J. Weidner (Am. Geophys. Union, Washington, D.C., 1989); J. Geophys. Res. **92**, 8116 (1987).